applied optics

Mid-infrared absorption-spectroscopy-based carbon dioxide sensor network in greenhouse agriculture: development and deployment

JIANING WANG,[1] LINGJIAO ZHENG,[1] XINTAO NIU,[1] CHUANTAO ZHENG,[1,2,*] YIDING WANG,[1,3] AND FRANK K. TITTEL[2]

[1]State Key Laboratory on Integrated Optoelectronics, College of Electronic Science and Engineering, Jilin University, Changchun 130012, China
[2]Electrical and Computer Engineering Department, Rice University, 6100 Main Street, Houston, Texas 77005, USA
[3]e-mail: ydwang@jlu.edu.cn
*Corresponding author: zhengchuantao@jlu.edu.cn

Received 17 June 2016; revised 26 July 2016; accepted 26 July 2016; posted 8 August 2016 (Doc. ID 268637); published 29 August 2016

A mid-infrared carbon dioxide (CO_2) sensor was experimentally demonstrated for application in a greenhouse farm environment. An optical module was developed using a lamp source, a dual-channel pyre-electrical detector, and a spherical mirror. A multi-pass gas chamber and a dual-channel detection method were adopted to effectively enhance light collection efficiency and suppress environmental influences. The moisture-proof function realized by a breathable waterproof chamber was specially designed for the application of such a sensor in a greenhouse with high humidity. Sensor structure of the optical part and electrical part were described, respectively, and related experiments were carried out to evaluate the sensor performance on CO_2 concentration. The limit of detection of the sensor is 30 ppm with an absorption length of 30 cm. The relative detection error is less than 5% within the measurement range of 30–5000 ppm. The fluctuations for the long-term (10 h) stability measurements on a 500 ppm CO_2 sample and a 2000 ppm CO_2 sample are 1.08% and 3.6%, respectively, indicating a good stability of the sensor. A wireless sensor network-based automatic monitoring system was implemented for greenhouse application using multiple mid-infrared CO_2 sensor nodes. A monitor software based on LabVIEW was realized via a laptop for real-time environmental data display, storage, and website sharing capabilities. A field experiment of the sensor network was carried out in the town of Shelin in Jilin Province, China, which proved that the whole monitoring system possesses stable sensing performance for practical application under the circumstances of a greenhouse.

OCIS codes: (130.0130) Integrated optics; (130.6010) Sensors; (120.0280) Remote sensing and sensors; (060.4250) Networks.

http://dx.doi.org/10.1364/AO.55.007029

1. INTRODUCTION

In recent years, ubiquitous agriculture, which is the combination of electrical technology [e.g., wireless sensor network (WSN), sensor] and agriculture, has been flourishing widely in Chinese agriculture [1–3]. The crop yield from solar greenhouses has increased by more than 3400 km^2 from 1820 to 2010 [4]. Due to the significant agricultural effects and the development of greenhouse farming, vertical farming with automatic management systems has gradually replaced the labor-intensive and extensive management in greenhouses.

In greenhouse farming, varying climatic and technological condition adjustments have a combined effect on the crop yield [4,5]. However, compared with the general greenhouse environmental parameters like temperature and humidity, relative study on gaseous fertilization (carbon dioxide, CO_2) technologies has not yet matured [4–6]. The official assessment report expects a yield increase of more than 20% because of the overall application effectiveness of gaseous CO_2 fertilizers [4]. Therefore, a cost-effective and field-deployable CO_2 sensor for the greenhouse environment becomes an urgent requirement.

Existing CO_2 sensing techniques normally include semiconductor, electrochemical, and infrared absorption spectroscopy [7–9]. In the special greenhouse environment, the mixed gases produced by crops and fertilizers limit the application of semiconductor sensors with low selectivity [7]. A large diurnal difference reduces the repeatability and stability of electrochemical sensors [8,9]. In contrast, the infrared absorption spectroscopy technique can satisfy various requirements, like wide measuring range, fast response, and high sensitivity [10–12].

Furthermore, the greenhouse environment has its own special working conditions and required detection range for CO_2. The existing infrared sensing techniques involve photoacoustic spectroscopy (PAS) [13], tunable diode laser absorption spectroscopy (TDLAS) [14–17], and direct absorption spectroscopy (DAS) [18]. PAS is one of the most famous spectroscopy techniques for trace gas detection because of its high sensitivity and selectivity. However, it is not suitable for *in situ* detection [13]. Although TDLAS has satisfying detection performance, the required cryogenic cooling of diode lasers is under a huge challenge because of the large diurnal difference in the greenhouse environment.

Consequently, due to the consideration of the trade-off between performance and cost, a low-cost mid-infrared CO_2 sensor (served as a node in the WSN) based on the DAS technique was designed and implemented in this paper to satisfy the greenhouse farm requirements. The proposed sensor is aimed at the desired performance for further reasonable CO_2 fertilization on yield increase. A spherical mirror served as a light collector was fabricated and integrated in the multi-pass gas chamber to enhance the light-collection efficiency. In order to satisfy the requirements of flexible installment and humidity protection in a greenhouse environment, a specially-designed breathable waterproof membrane was used to supply the ventilation duct between the outside and the chamber. In addition, as the data transmission channel, a wireless sensor network (WSN) was established based on multiple CO_2 sensor nodes to adequately display the dynamic changes in the whole greenhouse climate. An interactive interface based on LabVIEW for the greenhouse environment was developed. Design, measurement, and application of this monitoring system were performed in detail.

The main structure of this paper is organized as follows. In Section 2, structure and design of this sensor system are described. A WSN configuration and the related software are established to record and display the environmental data. In Section 3, a series of experiments are carried out in the laboratory and the corresponding results are given to evaluate this sensor system. In addition, a field deployment of this sensor network is performed to prove the function of this sensor system. Finally, in Section 4, some conclusions are reached.

2. SENSOR STRUCTURE AND DESIGN

A. Design Needs of the Sensor and WSN

With the development of the solar-greenhouse-based vegetable industry, CO_2 detection performance decides the effectiveness of gaseous CO_2 fertilizers in increasing crop yields directly. According to the practical conditions of greenhouses, such as intensity of photosynthesis and tightness of the greenhouse, there is a dynamic variation range of CO_2 concentration. However, the reasonable CO_2 concentration for vegetables should be between 500 and 2000 ppm, which is a relatively broad range in consideration of different results provided by related research [4,19]. This means that a real-time measurement and control on CO_2 concentration are desirable. In order to meet this special requirement, a large-range, real-time, and accurate measurement of CO_2 concentration based on WSN technology possesses an important role in increasing crop yields. The sensor should have a measurement limit of less than 100 ppm and be capable of wireless communication among all sensor nodes.

B. Sensor Node Structure

Figure 1 shows the schematic diagram of the developed mid-infrared CO_2 sensor, which includes an optical and an electrical part. In the optical part, the infrared light from a wideband infrared light source (IR55), is transmitted to a spherical reflector. After reflection, the infrared light is measured by a dual-channel infrared detector (LM242) with two sensing windows at 4.26 μm (with absorption) and at 4.00 μm (without absorption). According to the characteristics of blackbody heat source IR55, an aluminum block is glued with IR55 to prevent the spectral shift from cumulative temperature drift. In the process of light propagation, the emitted wideband infrared light propagates through the gas sample and is reflected onto the sensing surface of the detector. Because of the selective absorption of CO_2 molecules, the light passing through the 4.26 μm filter and the 4.00 μm filter will generate a detection signal and a reference signal, respectively. The electrical part mainly realizes three functions. The first function is a light source driver for supplying the desired driving signal to the light source. The second function is to perform the following signal processing functions, including pre-amplification (PA), band-pass filtering (BPF), lock-in amplifying, and analog-to-digital conversion (ADC). The last is a closed-loop feedback function. A 2.4 GHz wireless communication network is set up to transmit the data to a laptop terminal based on the LabVIEW interface for environmental-factor monitoring and data storage. Both the optical and electrical parts are controlled by a DSP (TI, type 28335) microprocessor because of its strong data-processing ability and pin alternate function.

C. Light Source and Detector

The used infrared light source (IR55) was fabricated with micro-electromechanical system (MEMS) technology with several advantages, such as a wide spectral range, low power consumption, and low cost. Equipped with two inherent filters, the PerkinElmer's dual-channel pyroelectric detector has a detectivity (D^*) of 3.5×10^8 cm $Hz^{1/2}$/W. Because of the received infrared light, the polarization of the material is changed due to temperature change, which generates a voltage difference, i.e., the original output signal from the detector. Before entering into the signal processing circuit, the signal is first processed by an inherent crystal and preamplifier in the detector. The wideband infrared emission from IR55 is modulated by a square-wave signal with a frequency of 4 Hz and a peak-to-peak current of 145 mA, because of the following two factors. First, because of the pyroelectric performance, the period of cooling and heating of the detector limits the modulation

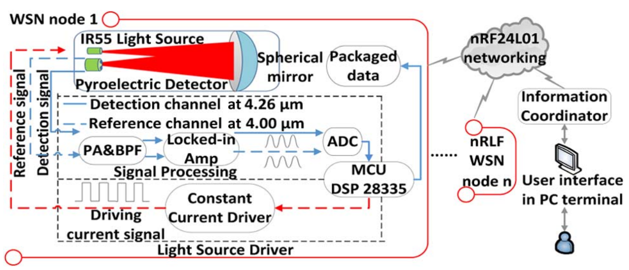

Fig. 1. Configuration of the mid-infrared CO_2 sensor network. The single sensor node includes an electrical and an optical part.

frequency to a low value. Regarding the 3 dB attenuation of the signal amplitude as the threshold, the modulation frequency is limited to 10 Hz. Second, a high modulation frequency in the infrared heart source IR55 will lead to the accumulation of heat. The combined effects of Doppler broadening and Lorentz broadening caused by temperature drift impacts the sensor precision. Therefore, a large-area cooling aluminum plate which has a good thermal conductivity was used to keep the temperature of the light source to a constant value.

The detailed absorption spectra of the CO_2 molecule within the two filter windows of the detector (at 4.26 and 4.00 μm) are shown in Fig. 2(a). The 4.26 μm window covers the strong absorption lines of CO_2, which are helpful for enhancing sensitivity. Also, CO_2 has extremely small absorption within the range of 3.9–4.0 μm, which can be used as a reference channel for background elimination. Based on Fig. 2(b), under 1 atm and 300 K, H_2O and CH_4 almost have no absorption within the two windows, so the two gases cause no effect on CO_2 detection.

The wideband radiance of the light source IR55, as shown in Fig. 3, covers the absorption wavelength of CO_2 molecules at 4.26 μm and reference wavelength at 4.00 μm. The spectrum was obtained from a Fourier transform infrared spectrometer (Thermo Fisher Scientific, model Nicolet Is50 FT-IR). The open-air measurement environment induces the absorption of CO_2 and H_2O in the spectra, as can be seen in Fig. 3.

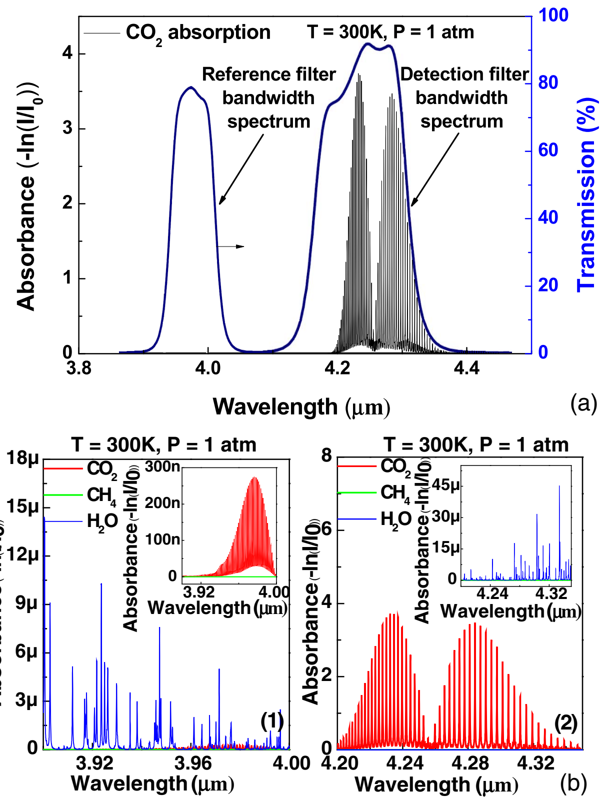

Fig. 2. (a) Absorption spectra of CO_2 at 4.26 and 4.0 μm as well as the two filter windows of the detector. (b) Absorption spectra of H_2O and CH_4 compared with CO_2 at (1) 4.0 μm and (2) 4.26 μm.

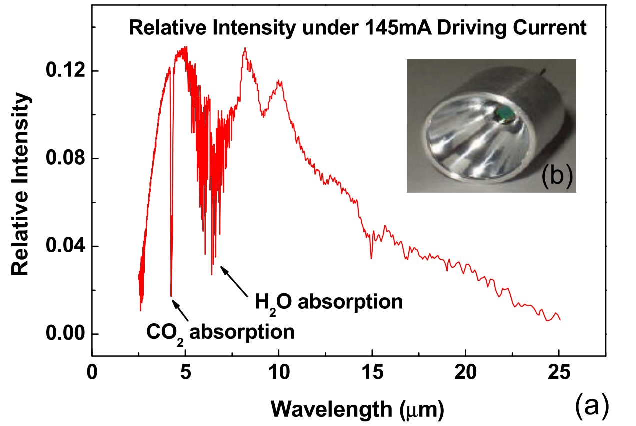

Fig. 3. (a) The emission spectrum and (b) the photo of the light source IR55.

D. Optical Path and Waterproof Design

A special spherical mirror was used as a light-collector. Define R, H, and D as its radius, height, and thickness, respectively, as marked in Fig. 4(b). Then the light-collection efficiency η can be calculated by the following formulas:

$$\eta = \begin{cases} \frac{\sqrt{R^2-(R-D)^2}}{R \sin \theta}, & (D < R(1-\cos \theta)) \\ 1, & (D \geq R(1-\cos \theta)) \end{cases}. \quad (1)$$

In order to enhance the light-collection efficiency under the consideration of both miniature size and easy integration, the relevant parameters of the aluminized spherical reflector were taken as $R = 200$ mm, $D = 10$ mm, and $H = 125$ mm. The photograph of the whole optical part is shown in Fig. 4(a). A fan was used to speed the gas diffusion into the chamber, as shown in Fig. 4(c).

In order to enable the application of such sensors in a greenhouse environment, several special constraints to the breathable waterproof membrane in greenhouse circumstances should be considered. Because of the diurnal temperature in a greenhouse, good capability at high humidity is a requirement. Still, because of the requirement of luminance measurement, the sensor should be exposed to high temperature caused by prolonged direct sunlight and the chemical corrosion from the fertilizer. In addition, the response time of the sensor depends on the permeability of the breathable waterproof membrane.

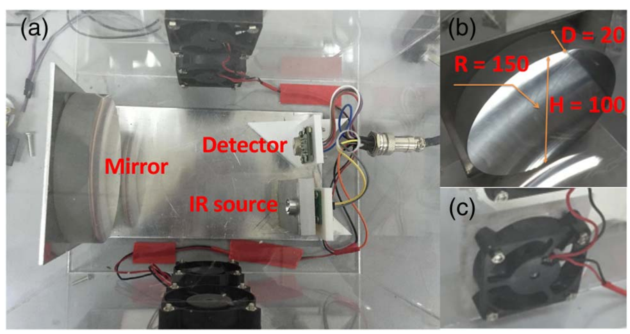

Fig. 4. (a) Photo of the optical part. (b) Photo of the spherical mirror. (c) Photo of the fan for gas injection to the chamber.

Therefore, a chamber was intensively designed for the above purposes or considerations, whose photo is shown in Fig. 4(a). There was a compromise selection between waterproof ability and breathability. The breathable waterproof membrane used in this sensor was made of expanded Polytetrafluoroethylene (ePTFE). The permeability of ePTFE is higher than 4 m/min, which has a superior performance to the commonly used material, thermoplastic polyurethanes (TPU). Furthermore, the high working temperature (up to 250°C) and chemical stability of ePTFE prevent influence from the special environmental circumstances of greenhouse. In addition, four fans were installed covering the breathable waterproof membrane to adjust the speed of air flow. Based on the above design and implementation, the sensor revealed a stable working condition under the protection of a breathable waterproof membrane in a greenhouse environment.

E. Differential Detection Structure and Theory

In consideration of the cost-effectiveness and practicability in a precision agriculture environment, the IR55, a wide-spectrum infrared light source, was used to emit the required optical radiation which covers the peak wavelength of the absorption band of CO_2. Two contrasting narrowband optical filters installed on the detector separated the received optical radiation into detection signal and reference signal, respectively. The central wavelengths of the two filter windows at 4.26 and 4.00 μm correspond to the absorption region of CO_2 and non-absorption region of CO_2, respectively. The received optical radiation through different optical filters with the same prerequisites like source, transmission path, and delay were performed for differential operation to suppress the interferences from the sensor itself and from environmental factors. The used dual-channel differential detection method enhances gas measurement accuracy and reduces the maintenance period.

The Beer–Lambert law could be formulated as

$$I = I_0 \exp(-KCL), \tag{2}$$

where I is the light intensity received by the two filtering windows, I_0 is the initial emitting light intensity, K is the absorption coefficient, C is the CO_2 concentration, and L is the optical length.

In consideration of the agricultural greenhouse environment and scattering influence, the Raleigh scattering, Mie scattering, and absorption of water vapor should be formulated theoretically. However, since the two filter peak wavelengths $\lambda_1 = 4.26$ μm and $\lambda_2 = 4.00$ μm are too close to each other, the Raleigh scattering coefficient and Mie scattering coefficient at these two wavelengths are nearly the same. After the calculation of differential ratio signal $\Delta U/U_2$, the scattering and absorption coefficients could be eliminated, which was already proved in a previous work [17]. Therefore, the final CO_2 concentration could be expressed as

$$C = \frac{1}{KL} \ln\left[\frac{k_1}{k_2}\left(1 - \frac{\Delta U}{U_2}\right)\right]. \tag{3}$$

In Eq. (3), k_1 and k_2 are the relative optical-to-electrical conversion coefficients at λ_1 and λ_2, respectively, ΔU is the difference between the amplitude (U_1) of the detection signal and the amplitude (U_2) of the reference signal. Such relation can be obtained through calibration experiment.

F. Wireless Communication and PC Software

A wireless sensor network was proposed to set up the communication among the multiple sensor nodes because of the difficulty in wired communication. Compared with other wireless modules, like ZigBee and Bluetooth, nRF24L01, which was integrated in the sensor, has the advantages of long transmission distance, low power consumption, and flexible installment. Data communication and command transmission only depends on two IO pins, which frees us from complicated sensor integration. A multiple-to-one communication mode, maximum six to one, satisfies the multi-simultaneous communication requirement and reduces the channel blockage time.

In this wireless sensor network, after a communication channel was established, the Received Signal Strength Indication (RSSI) was measured following the collected data transmission to evaluate the quality of the wireless communication signal, implying the wireless communication performance. According to the datasheet of NRL24L01, the reference deadline RSSI is −95 dBm, indicating that when the RSSI value is lower than −95 dBm, the signal is considered invalid. In addition, in consideration of the multiple sensor nodes in the same wireless communication frequency range installed in a greenhouse, the RSSI value should not be too high to avoid co-channel interference. Under the comprehensive consideration, the reasonable RSSI value range was set to −70 dBm to −90 dBm. The several selective working powers like 0, −10, and −20 dBm, would be smart-regulated based on the measured RSSI value. The related network communication field experiments were carried on in a greenhouse, which will be discussed in the following experiment part.

The server based on LabVIEW is a system-design platform and a development environment for this application. The graphical user interface (GUI) based on LabVIEW supports powerful function libraries and comprehensive graphical tools to realize the interactive data acquisition and instrumental control applications. The virtual instrument modulated by LabVIEW is famous for its scalability, modularity, and customization. Dependent on those advantages, multithreading data transmission and control applications were realized. For data transmission, both universal asynchronous receiver/transmitter (UART) and wireless communication were available to cope with a variety of applications. Besides CO_2 concentration, temperature, humidity, and luminance were sampled as the relevant environmental factors to calibrate the CO_2 concentration data by software. The link between the SQL database and LabVIEW format was established and the sampled data was real-time recorded for further analysis. The storage path could be set in the selection box in the front monitoring panel. The relevant storage details were done automatically in the background subroutines. The real-time monitoring window graphs showed the recent variation trend of the selected environmental factor(s). The interface software also realized the local and web application. With the related software terminals, users can monitor the real-time detected environmental information through a browser.

3. EXPERIMENTAL RESULTS

A. Gas Experiment Preparation

To get a stable and accurate calibration result, dynamic gas distribution was used in a gas experiment instead of the static injection distribution via a needle. The 5000 ppm CO_2 samples with 2% uncertainty and 99.999% pure N_2 were used as gas sources. Different CO_2 concentrations were prepared by mixing the above two gases through a mass flow meter (MT50-3G). The preparation rule is written as

$$C = \frac{V_1 \times 5000\ \text{ppm}}{V_1 + V_2}. \tag{4}$$

In the above formula, C is the required CO_2 concentration and V_1 and V_2 are the required volumes of the standard CO_2 sample and pure N_2, respectively.

B. System Noise and Calibration Experiment

A high signal-to-noise ratio (SNR) indicates a high accuracy and a low detection limit of the sensor. The noise characteristics of the sensor under both the turn-on state and turn-off state of the light source were measured using a radio-frequency spectrum analyzer. Under the turn-on state, the frequency and time-domain characterization of the amplified signals output from the detection channel and reference channel are shown in Figs. 5(a) and 5(b), respectively. The main noise is white noise, whose power spectral density is uniformly distributed throughout the frequency domain. The sensor was powered by a switching power supply, yet the power frequency interference (lower than −50 dB) at 50 Hz is not significant. The average noise magnitudes in both detection and reference channel were about −65 dB, which are not able to influence the detection performance. Note that during the experiment, pure N_2 was kept flushing into the chamber for maintaining a zero-CO_2 concentration.

When the light source was modulated by a square-wave signal with a frequency of 4 Hz, the measured frequency responses of the two output signals from the detection channel and reference channel are shown in Figs. 6(a) and 6(b), respectively. Both the detection and reference channel have satisfying signal-to-noise ratios (SNR) at 4 Hz. And the 10 dB bandwidth is ~2 Hz at 4 Hz frequency, indicating a good performance of this sensor.

In the calibration experiment, a series of gas samples with different concentration levels distributed by the mass flow meter was prepared and kept flushing the chamber, and the amplitude of the output signal from the detection channel (U_1) and the amplitude from the reference channel (U_2) were recorded for 30 min until the readings were stable. The measurement results of ΔU over a time period of 10 min for each concentration are shown in Fig. 7(a). The averaged value of ΔU was obtained and used to represent the corresponding concentration. The relationship curves between the averaged ΔU and concentration C are shown in Fig. 7(b). The curve was fitted by

$$C = 43.424 - 1779.38 \ln\left(\frac{0.20008 - \Delta U}{1.3698}\right). \tag{5}$$

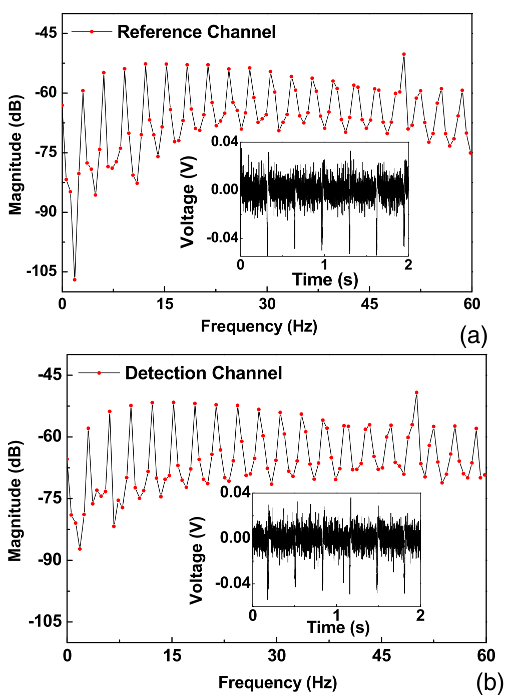

Fig. 5. When the infrared light source is set to the turn-off state with a CO_2 concentration of 0 ppm, the measured time and frequency-domain signal output from (a) detection channel and (b) reference channel after pre-amplifier. The insets in the two figures are the relevant time-domain signals.

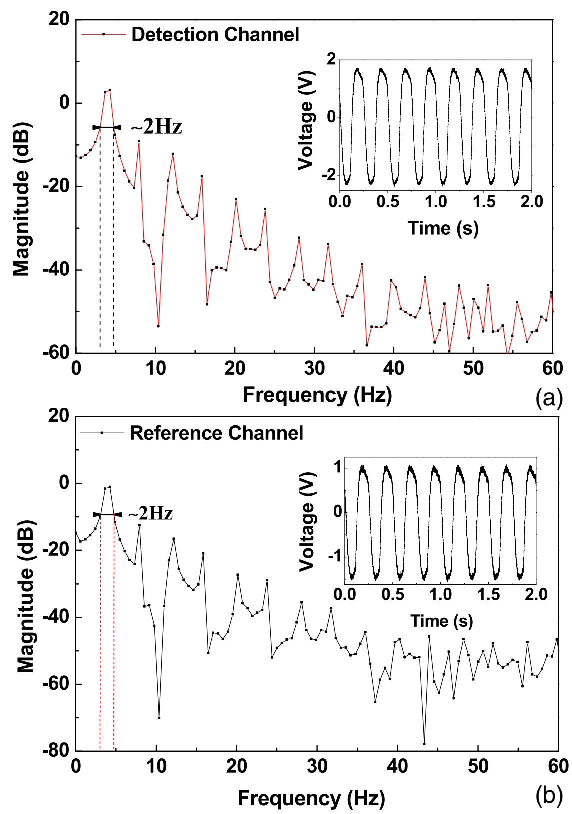

Fig. 6. When the infrared light source is modulated at 4 Hz, the measured spectra of the (a) detection channel and (b) reference channel from pre-amplifier. The insets in the two figures are the relevant time-domain signals.

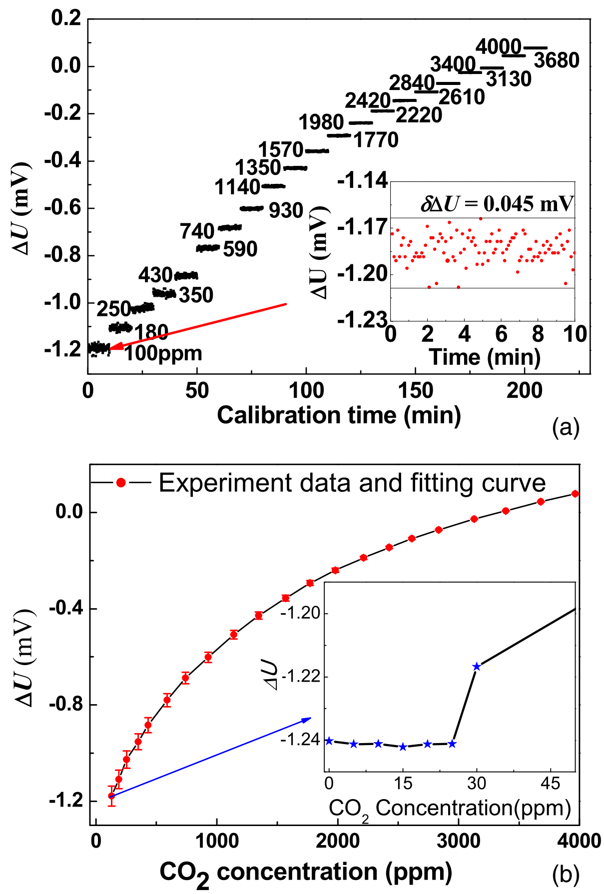

Fig. 7. (a) Experimental data dots of the differential ratio (ΔU) versus the standard CO_2 concentration. The inset shows the measured ΔU under 100 ppm for 10 min. (b) Experimental data dots and fitting curve of the measured differential ratio versus the distributed standard CO_2 concentration. The inset shows the LoD measurement results.

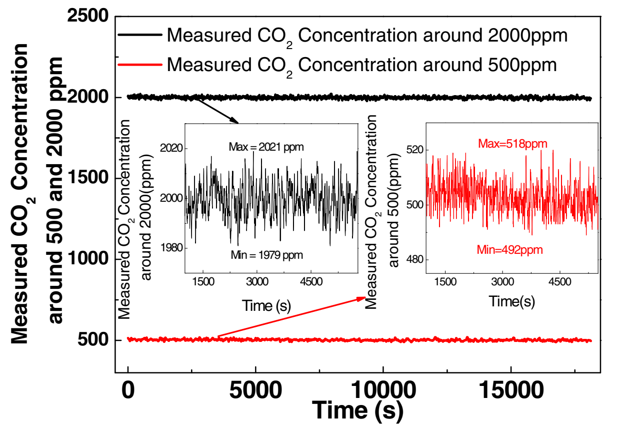

Fig. 8. Long-term measurement results on the two CO_2 standard samples with concentration levels of 500 and 2000 ppm.

In the limit of detection (LoD) measurement, after the chamber was flushed by pure N_2, CO_2 mass flow was increased slowly until a minimum peak-to-peak output voltage ratio increase can be observed steadily. The stable CO_2 concentration reading under this situation was 30 ppm as shown in the inset in Fig. 7(b). In consideration of the CO_2 concentration in the atmosphere and the limited sealing performance in the greenhouse environment, the performances mentioned above were acceptable. After calibration, the concentration reading from this sensor agreed well with the standard concentration distributed by the mass flow meter.

C. Detection Stability

In stability measurement, the sample gases distributed by the mass flow meter kept flushing the chamber at a slow flow rate to make sure there was a stable and accurate CO_2 concentration in the chamber. In consideration of the application environment in a greenhouse, the two diluted CO_2 concentration levels were 500 and 2000 ppm, which are the normal CO_2 concentration and desired CO_2 concentration in a greenhouse, respectively. Because of the noises and interference in the system, there are acceptable fluctuations of 1.08% (21/2000) and 3.6% (18/500) of the measurement results on the 2000 and 500 ppm samples, respectively, as shown in Fig. 8.

The detection sensitivity is the ratio between the change in the detector output signal and the change of the measured concentration. A larger ratio indicates a more sensitive sensor system. In this experiment, the concentration of each CO_2 sample was increased by 30 ppm within the range of

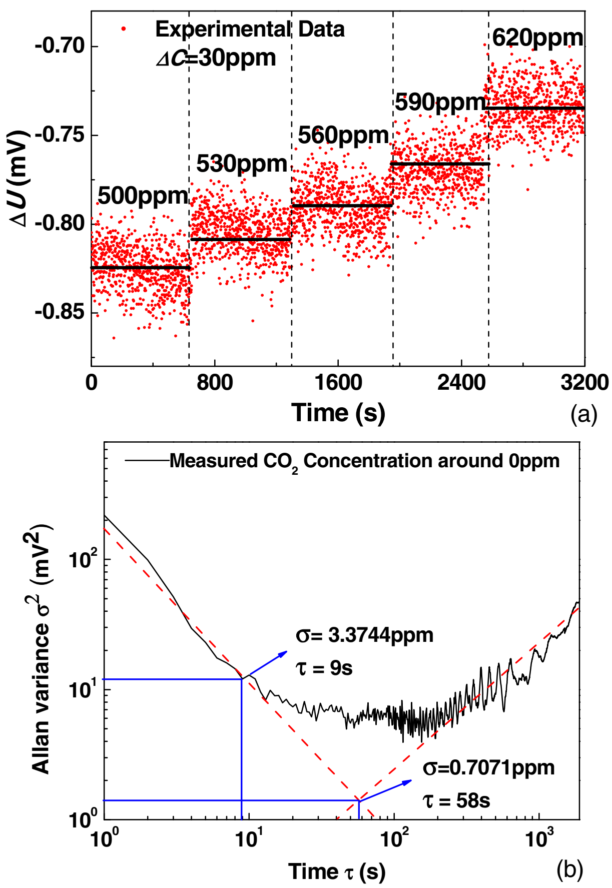

Fig. 9. (a) Measurement results of the detection sensitivity in the range from 500–620 ppm. (b) Allan variance plot of this sensor at a pure N_2 atmosphere.

500–620 ppm. Such range is the common CO_2 concentration range in a greenhouse without deliberate human interference. The prepared standard gas samples kept flushing the chamber and the data was recorded after the reading was stable. The related results are shown in Fig. 9(a). The detection sensitivity of the sensor was <30 ppm.

Figure 9(b) shows the Allan variance of this sensor, indicating the stability performance and theoretical detection limitation of this system [20]. A long-term evaluation of this sensor was done in a pure N_2 environment. From the Allan variance result, the white noise ends at a 9 s integration time where the slope differs from −1. The responding theoretical detection limit is 3.3744 ppm. If the integration time keeps increasing until reaching the intersection point of the 1/2 slope, the Allan variance is much lower at an integration time of 58 s at the price of system response speed. If the integration time keeps increasing until the integration time is 60 s, the Allan variance becomes much lower at the price of sensor response speed. Under this situation, the main noise comes from the system drift of temperature or some environmental influences. In the greenhouse environment, it should be appropriate to increase the integration time to a reasonable value to enhance the stability of this sensor.

D. Sensor Network Regulation Based on RSSI Measurement

The CO_2 sensor network was placed in an 8×84 m^2 cucumber greenhouse. Because of the requirement of different spatial location measurement, the different transmission distance and the consequent influence were inevitable and worth considering. The sensor network communication experiments were carried out in a greenhouse and the relative RSSI values were calculated. The wireless communication module was powered by a standard 5 V voltage and the matched antenna was a common single whip type. The transmission power was set to 0 dBm (1 mW), which would be amplified by the following ratio-frequency amplified chip to 14 dBm (25 mW). As shown in Fig. 10, in the communication experiment, the test results were basically consistent with the theoretical anti-exponential curve, including some fluctuation points caused by the regional plant shelter and inherent fluctuation. When the standard RSSI value was at the range of −70 to −90 dBm, the acceptable transmission distance is 20 to 78 m, which is able to satisfy the greenhouse application. The test results were measured in the germination period of the plants, and there would be more signal attenuation in the harvest period because of the relative strong plant shelter influence to the transmission signal. According to the different growth stages of certain plants, the measurement nodes in the sensor network intelligently adjusted the transmission power to optimize the transmission performances, including ensuring signal quality, saving power, and avoiding co-channel interference.

E. Field Experiment

In order to prove the application ability of this sensor in a greenhouse, some field experiments were carried out in the town of Shelin in Jilin Province. The breathable waterproof

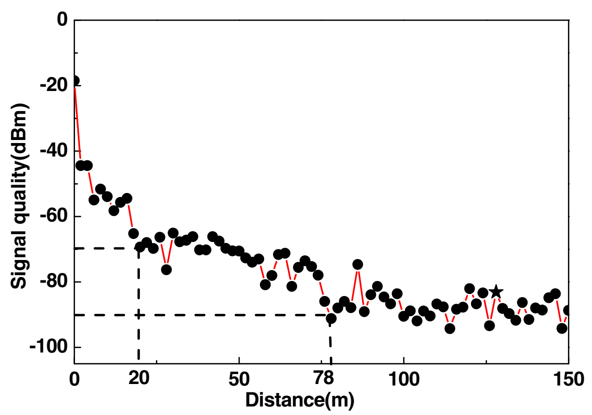

Fig. 10. Measured RSSI value with increasing communication distance in greenhouse.

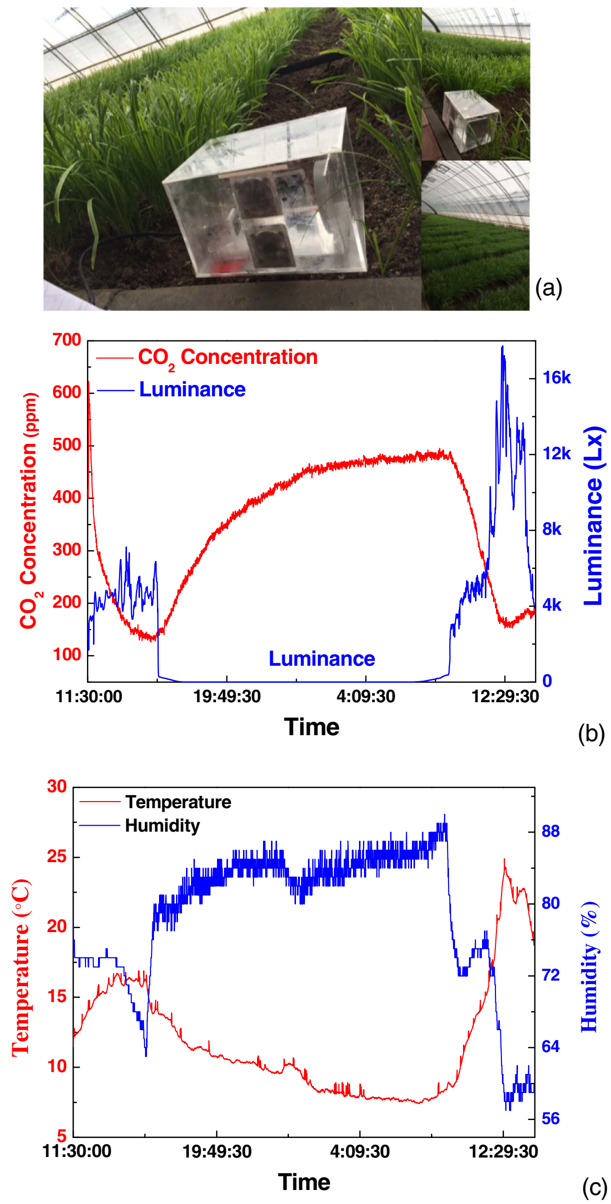

Fig. 11. (a) Photo of the leek solar greenhouse as well as a plastic box with a CO_2 sensor node inside. (b) Measured CO_2 concentration and luminance data in the greenhouse. (c) Measured temperature and humidity data in the green house.

membrane with fans installed in the optical part had a good performance in breathability and moisture resistance. The stable and accurate performance of the sensor indicated that the breathable waterproof membrane prevented influence from the special environmental conditions of a greenhouse. Similarly, the data cables were connected outside of the greenhouse through air plugs to prevent influence from the high humidity on the interface between the optical part and the electrical part. The field installation and environmental measurement data are shown in Figs. 11(a)–11(c).

The monitoring results in the leek solar greenhouse above were compliant with photosynthesis law, indicating that there were no detection errors during the field test. The greenhouse CO_2 concentration arrived to its lowest value of 168 ppm at nearly 1:00 pm with the highest temperature of 23°C. At 3:30 pm, the rolling machines were driven to cover the ceiling of the greenhouse for temperature insulation, which was the reason why the luminance reduces to zero drastically. In addition, the reasonable compensation of CO_2 gas fertilization corresponding to the plant species and growth stage was a potential application based on the proposed sensor system.

As a result of applying the proposed sensor system to the leek solar greenhouse, sufficient environmental information was sampled in several methods, such as database, SD card, local GUI, and website broadcast, which are intuitive for users to monitor and analyze the greenhouse conditions.

4. CONCLUSION

A greenhouse farm monitoring system based on a differential mid-infrared CO_2 concentration sensor was implemented. The used compact moisture-proof chamber and single-source dual-channel detection system ensured adaptability and stability in the special greenhouse environment. The relationship between the desired CO_2 concentration and measured amplitudes of the two channels was obtained, and related experiments were carried out to characterize the instrument performance. The detection limit on CO_2 concentration is lower than 30 ppm, and the detection error in the range of 100 to 1500 ppm, which is the common range in greenhouse, is less than 2%. Besides the CO_2 sensor, some key modules, including a WSN and a monitoring platform based on LabVIEW, were realized. The stability and reliability of communication via the WSN was satisfied based on the RSSI measurement, and the relative smart transmission power regulation was adopted corresponding to different stages of plant growth. The proposed monitoring sensor system shows desirable performance in the practical field experiments.

Funding. National Key Technology R&D Program of China (2014BAD08B03, 2013BAK06B04); National Natural Science Foundation of China (NSFC) (61307124, 11404129); Science and Technology Department of Jilin Province of China (20120707, 20140307014SF); Changchun Municipal Science and Technology Bureau (11GH01, 14KG022); State Key Laboratory of Integrated Optoelectronics, Jilin University (IOSKL2012ZZ12).

REFERENCES

1. J. Hwang, C. Shin, and H. Yoe, "A wireless sensor network-based ubiquitous paprika growth management system," Sensors **10**, 11566–11589 (2010).
2. A. Somov, A. Baranov, D. Spirjakin, A. Spirjakin, V. Sleptsov, and R. Passerone, "Deployment and evaluation of a wireless sensor network for methane leak detection," Sens. Actuators A **202**, 217–225 (2013).
3. A. Somov, A. Baranov, and D. Spirjakin, "A wireless sensor-actuator system forhazardous gases detection and control," Sens. Actuators A **210**, 157–164 (2014).
4. M. Xin, L. Shuang, L. Yue, and G. Qinzhu, "Effectiveness of gaseous CO_2 fertilizer application in China's greenhouses between 1982 and 2010," J. CO_2 Util. **11**, 63–66 (2015).
5. J. Hwang, C. Shin, and H. Yoe, "Study on an agricultural environment monitoring server system using wireless sensor networks," Sensors **10**, 11189–11211 (2010).
6. A. Malaver, N. Motta, P. Corke, and F. Gonzalez, "Development and integration of a solar powered unmanned aerial vehicle and a wireless sensor network to monitor greenhouse gases," Sensors **15**, 4072–4096 (2015).
7. A. V. Salker, N.-J. Choi, J.-H. Kwak, B.-S. Joo, and D. Lee, "Thick films of In, Bi and Pd metal oxides impregnated in $LaCoO_3$ perovskite as carbon monoxide sensor," Sens. Actuators B **106**, 461–467 (2005).
8. S. C. K. Misra, P. Mathur, and B. K. Srivastava, "Vacuum-deposited nanocrystalline polyaniline thin film sensors for detection of carbon monoxide," Sens. Actuators A **114**, 30–35 (2004).
9. R. J. Wu, C. H. Hu, C. T. Yeh, and P. G. Su, "Nanogold on powdered cobalt oxide for carbon monoxide sensor," Sens. Actuators B **96**, 596–601 (2003).
10. Y. Cao, N. Sanchez, W. Jiang, R. J. Griffin, F. Xie, L. C. Hughes, C. Zah, and F. K. Tittel, "Simultaneous atmosphere nitrous oxide, methane and water vapor detection with a single continuous wave quantum cascade laser," Opt. Express **23**, 2121–2132 (2015).
11. C. Chen, R. W. Newcomb, and Y. D. Wang, "A trace methane gas sensor using mid-infrared cascaded laser at 7.5 μm," Appl. Phys. B **113**, 491–501 (2013).
12. J. Hodgkinson, R. Smith, W. Ho, J. Saffell, and R. Tatam, "A low cost, optically efficient carbon dioxide sensor based on nondispersive infrared (NDIR) measurement at 4.2 μm," Proc. SPIE **8439**, 843919 (2012).
13. T. Chen, G. F. Su, and H. Y. Yuan, "In situ gas filter correlation: photoacoustic CO detection method for fire warning," Sens. Actuators B **109**, 233–237 (2005).
14. C. T. Zheng, W. L. Ye, J. Q. Huang, T. S. Cao, M. Lv, J. M. Dang, and Y. D. Wang, "Performance improvement of a near-infrared CH_4 detection device using wavelet-denoising-assisted wavelength modulation technique," Sens. Actuators B **190**, 249–258 (2014).
15. B. Li, C. T. Zheng, H. F. Liu, Q. X. He, W. L. Ye, Y. Zhang, J. Q. Pan, and Y. D. Wang, "Development and measurement of a near-infrared CH_4 detection system using 1.654 μm wavelength-modulated diode laser and open reflective gas sensing probe," Sens. Actuators B **255**, 188–198 (2016).
16. A. Pogány, O. Ott, O. Werhahn, and V. Ebert, "Towards traceability in CO_2 line strength measurements by TDLAS at 2.7 μm," J. Quant. Spectrosc. Radiat. Transfer **130**, 147–157 (2013).
17. G. L. Li, Y. Sui, M. Dong, W. L. Ye, C. T. Zheng, and Y. D. Wang, "A carbon monoxide detection device based on mid-infrared absorption spectroscopy at 4.6 μm," Appl. Phys. B **119**, 287–296 (2015).
18. A. Thompson, H. Northern, B. Williams, M. Hamilton, and P. Ewart, "Simultaneous detection of CO_2 and CO in engine exhaust using multi-mode absorption spectroscopy, MUMAS," Sens. Actuators B **198**, 309–315 (2014).
19. S.-H. Yang, C. G. Lee, A. Ashtiani-Araghi, J. Y. Kim, and J. Y. Rhee, "Development and evaluation of combustion-type CO_2 enrichment system connected to heat pump for greenhouses," Eng. Agric. Environ. Food **7**, 28–33 (2014).
20. G. J. Tu, F. Z. Dong, Y. Wang, B. Culshaw, Z. Zhang, T. Pang, H. Xia, and B. Wu, "Analysis of random noise and long-term drift for tunable diode laser absorption spectroscopy system at atmospheric pressure," IEEE Sens. J. **15**, 3535–3542 (2015).